Available online at www.sciencedirect.com
SCIENCE DIRECT
International Journal of Heat and Mass Transfer 49 (2006) 3111–3120
International Journal of HEAT and MASS TRANSFER
www.elsevier.com/locate/ijhmt

Soret effect on the boundary layer flow regime in a vertical porous enclosure subject to horizontal heat and mass fluxes

M. Er-Raki [a], M. Hasnaoui [a,*], A. Amahmid [a], M. Mamou [b]

[a] Faculty of Sciences Semlalia, Department of Physics, B.P. 2390, Marrakesh, Morocco
[b] Institute for Aerospace Research, National Research Council, Ottawa, Ont., Canada K1A 0R6

Received 6 September 2005; received in revised form 10 February 2006
Available online 18 April 2006

Abstract

The combined thermo- and double-diffusive convection in a vertical tall porous cavity subject to horizontal heat and mass fluxes was investigated analytically and numerically using the Darcy model with the Boussinesq approximation. The investigation focused on the effect of Soret diffusion on the boundary layer flow regime. The governing parameters were the thermal Rayleigh number, R_T, the Lewis number, Le, the buoyancy ratio, N, the Soret parameter, M, which characterized the Soret effect, and the aspect ratio of the enclosure, A_r. The results demonstrated the existence of a boundary layer flow solution for which the Soret parameter had a strong effect on the heat and mass transfer characteristics. For $M \neq 1$ and $M \neq -1/Le$, the profiles of the vertical velocity component, v, temperature, T, and solute concentration, S, exhibited boundary layer behaviors at high Rayleigh numbers. Furthermore, as R_T increased, the temperature and solute concentration became vertically and linearly stratified in the core region of the enclosure. The thermo-diffusion effect on the boundary layer thickness, δ, was discussed for a wide range of the governing parameters. It was demonstrated analytically that the thickness of the boundary layer could either increase or decrease when the Soret parameter was varied, depending on the sign of the buoyancy ratio. The effect of R_T on the fluid flow properties and heat and mass transfer characteristics was also investigated.

Keywords: Vertical porous enclosure; Heat and mass transfer; Thermo-solutal convection; Soret effect; Boundary layer; Analytical and numerical studies

1. Introduction

The combined thermo-diffusive and double-diffusive convection in a fluid-saturated porous media is of practical interest in many engineering applications such as petrology, hydrology, solidification of binary alloys, as well as many other applications. This phenomenon occurs when a temperature gradient induces a transfer of solute, whether in the presence or in the absence of a solute concentration gradient. Depending on the nature of the fluid mixture, the solute migration can occur towards the heated or cooled regions. A literature review showed that the phenomenon leads to various and complex flow patterns, especially when the thermal and solutal buoyancy forces oppose each other and are of the same order of magnitude. This particular phenomenon has attracted many researchers in various thermo-fluid, chemical and metallurgical disciplines, and remains a hot subject of the decade. Most previous studies are related to rectangular flow configurations with impermeable boundaries for mass transfer. When such configurations are submitted to vertical temperature gradients, attention is generally focused on flow stability and bifurcation problems.

Bénard convection of a binary liquid in a porous medium was investigated by Karcher and Müller [1]. Using a two-parameter perturbation analysis, the Soret effect on the stability of the basic state and finite-amplitude convection was determined. These authors found that a nonlinear density–temperature relationship has a destabilizing effect on the conductive regime. A numerical study of the Soret effect on multiple steady-state solutions, induced by

* Corresponding author. Tel.: +212 24 43 46 49; fax: +212 24 43 74 10.
E-mail address: hasnaoui@ucam.ac.ma (M. Hasnaoui).

0017-9310/$ - see front matter © 2006 Elsevier Ltd. All rights reserved.
doi:10.1016/j.ijheatmasstransfer.2006.02.028

Nomenclature

A_r	aspect ratio of the porous matrix, H'/L'
D	mass diffusivity of the species
D_T	thermo-diffusion coefficient
g	gravitational acceleration
H'	height of the enclosure
j'	constant mass flux per unit area
K	permeability of the porous medium
L'	thickness of the enclosure
Le	Lewis number, α/D
M	Soret parameter, $S'_0 D_T \Delta T'/(D\Delta S')$
N	buoyancy ratio, $\beta_S \Delta S'/\beta_T \Delta T'$
Nu	Nusselt number, Eq. (7)
q'	constant heat flux per unit area
R_T	thermal Darcy–Rayleigh number, $g\beta_T K q' L'^2/(\lambda\alpha\nu)$
S	dimensionless solute concentration, $(S' - S'_0)/\Delta S'$
S'_0	reference solute concentration
Sh	Sherwood number, Eq. (7)
$\Delta S'$	characteristic solute concentration, $j'L'/D$
t	dimensionless time, $t'\alpha/(L'^2\sigma)$
T	dimensionless temperature, $(T' - T'_0)/\Delta T'$
T'_0	reference temperature
$\Delta T'$	characteristic temperature, $q'L'/\lambda$
(u, v)	dimensionless velocities in the (x, y) directions, $(u'L'/\alpha, v'L'/\alpha)$
(x, y)	dimensionless coordinates, $(x'/L', y'/L')$

Greek symbols

α	thermal diffusivity
β_S	solute concentration expansion coefficient
β_T	thermal expansion coefficient
ε	normalized porosity, ε'/σ
ε'	porosity of the porous medium
λ	thermal conductivity
ν	kinematic viscosity of the fluid
ρ	density of the fluid mixture
ρ_a	dimensionless density of the fluid, $-(T + NS)$
$(\rho c)_f$	heat capacity of the fluid mixture
$(\rho c)_p$	heat capacity of the saturated porous medium
σ	heat capacity ratio, $(\rho c)_p/(\rho c)_f$
ψ	dimensionless stream function, ψ'/α
ζ	dimensionless vorticity, $\zeta' L'^2/\alpha$
η	relaxation factor, $(C_a K\alpha)/(\sigma L'\nu)$

Superscript

$'$	dimensional variable

Subscripts

max	maximum value
min	minimum value
0	reference state
S	solutal
T	thermal

double-diffusive convection in a square porous cavity, submitted to cross gradients of temperature and concentration was performed by Mansour et al. [2]. Depending on the value of the Soret parameter, up to three convective solutions were found to be possible and their domains of existence were delimited. Bourich et al. [3] investigated the Soret effect on natural convection in a horizontal porous layer heated from below and cooled from above with uniform fluxes of heat. Critical conditions for the onset of subcritical and stationary convection were determined analytically in the limit of a shallow enclosure. The onset of Soret-driven convection in an infinite porous layer with horizontal walls maintained at different and uniform temperatures was investigated by Sovran et al. [4]. The criteria for the onset of motion via stationary and Hopf bifurcations were derived for cases dealing with heating from below or above. The authors showed that the bifurcation from the rest state depended, among other parameters, on the separation ratio. Soret driven thermo-solutal convection in a shallow Brinkman porous layer, with a stress-free upper surface, subject to constant fluxes of heat on its horizontal walls was studied analytically and numerically by Er-Raki et al. [5]. It was found that the Soret effect can play a stabilizing or a destabilizing role and this, depending on the sign of the separation parameter. Supercritical and subcritical Rayleigh numbers were determined as a function of the parameters governing the problem. Double-diffusive and pure Soret effect natural convection induced in a horizontal porous layer was investigated analytically and numerically by Bahloul et al. [6]. A linear stability analysis of the parallel flow pattern was used to determine the critical conditions corresponding to the onset of convection thresholds. The occurrence of finite-amplitude, oscillatory and monotonic convection instabilities were predicted. Alex and Patil [7] studied the effect of the gravity gradient on the onset of thermo-solutal convection due to thermal diffusion in a fluid saturated porous layer with horizontal boundaries maintained at constant but different temperatures and solute concentrations. The results showed that the pattern of the convective flow was affected by the Soret parameter only when its magnitude was sufficiently large. Recently, the Soret effect on thermo-solutal convection induced in a horizontal Darcy porous layer subject to constant heat and mass fluxes was the object of analytical and numerical studies by Bourich et al. [8]. The thresholds for the onset of supercritical and subcritical convection were predicted explicitly as functions of the governing parameters. It was demonstrated that there existed combinations of the governing parameters for which the Soret effect imposed a vertical non-linear stratification of

the concentration gradient even for a convective flow regime. A reversal of the horizontal concentration gradient was also possible. Soret-driven thermo-solutal convection within a shallow porous layer subject to a vertical temperature gradient was investigated analytically and numerically by Bourich et al. [9]. They performed a comparative study for Darcy porous and clear fluid media. The onset of overstability was predicted using a linear stability analysis. An appropriate normalization for the Rayleigh number was used to demonstrate that the flow behavior for any aspect ratio of the enclosure was similar to that predicted by the parallel flow assumption.

In the case of vertical porous enclosures, the Soret effect has also been the object of study. Hence, Soret induced thermo-gravitational diffusion within a rectangular vertical porous cavity subjected to horizontal thermal gradients was considered by Marcoux et al. [10]. The case of opposing and equal thermal and solutal buoyancy forces was considered. A linear stability analysis of the purely diffusive state was performed and the thresholds of instability were computed for various aspect ratios of the enclosure. The problem of thermal diffusion in an initially homogeneous mixture submitted to a horizontal thermal gradient was studied experimentally and numerically by Benano-Melly et al. [11]. The numerical results showed that, depending on the Soret number, multiple convective flow patterns were possible in the case of counteracting solutal and thermal buoyancy forces. Joly et al. [12] studied analytically and numerically the Soret effect on the onset of natural convection within a vertical porous layer subject to uniform heat fluxes on its vertical walls using the Brinkman–extended Darcy model. The case of opposing solutal and thermal buoyancy forces with the same magnitude was considered. A linear stability analysis was used to study the stability of small perturbations from the rest state. The dependence of the supercritical Rayleigh number on the aspect ratio of the enclosure and the Darcy number was found to be similar to that obtained in the case of a double-diffusive problem in a layer subject to equal and opposite vertical buoyancy forces and horizontal gradients of heat and mass. However, the supercritical Rayleigh number dependence on the Lewis number was different for the two problems.

In the present study, the Soret effect on the double-diffusive convective flows inside a vertical porous layer subject to horizontal heat and mass fluxes was studied analytically and numerically. In a related subject, Boutana et al. [13] investigated analytically and numerically the problem of natural convection induced in a vertical porous layer filled with a binary fluid. Two different situations had been examined by these authors. The first situation corresponded to a double-diffusive natural convection in a vertical enclosure submitted to horizontal heat and mass fluxes where the Soret effect was neglected, and the second one concerned a pure Soret convection induced by imposed temperature gradient (constant heat flux). For a negative separation ratio close to -1, multiple convective solutions with different flow patterns were found to exist and the characteristics of the boundary layer regime were investigated. In the present study, the two situations examined by Boutana et al. [13] can be recovered as limiting cases in the mathematical formulation.

The aim of the present paper consists in studying the influence of the Soret effect on thermal and solutal boundary layers induced in a vertical porous matrix obeying the Darcy law and subject to horizontal heat and mass fluxes. The boundary layer flow regime was investigated in the absence of the Soret effect under various thermal and solutal boundary conditions by Trevisan and Bejan [14,15], Alavyoon [16] and Amahmid et al. [17]. In the present work, a Soret parameter was introduced in the governing equations to characterize the thermo-diffusion phenomenon. Within the boundary layer flow regime, the combined effect of the Soret and other governing parameters of the problem was investigated.

2. Problem formulation

The physical model under study is sketched in Fig. 1. The model was represented by a tall vertical porous layer that consisted of an isotropic, homogeneous and saturated Darcy porous medium. The size of the porous layer was defined by an aspect ratio $A_r = H'/L' \gg 1$, where H' and L' are the height and the width of the layer. The top and bottom end walls of the layer were assumed adiabatic and impermeable to mass transfer while the two long side walls were subject to uniform fluxes of heat, q', and mass,

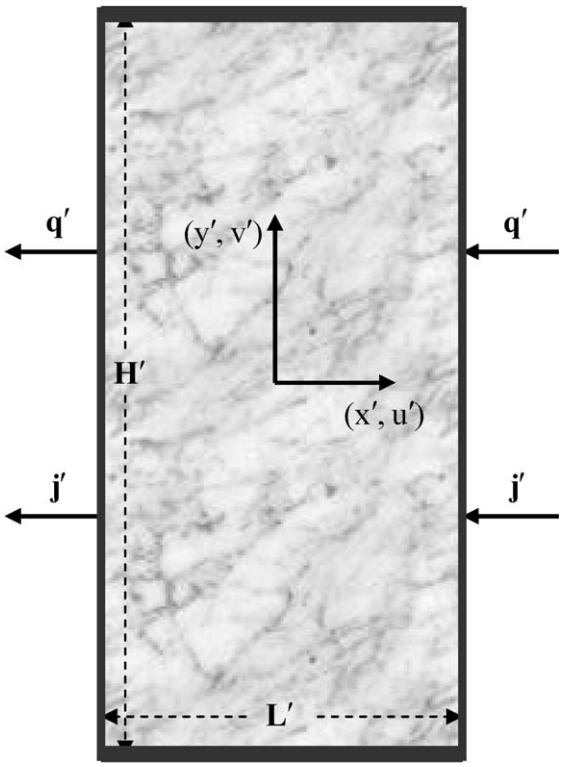

Fig. 1. Schematic of the physical system.

j'. The coordinate system origin was chosen at the center of the cavity. The diluted binary fluid that saturated the porous medium was modeled as a Boussinesq incompressible fluid for which the fluid density varied according to the relationship given by $\rho = \rho_0[1 - \beta_T(T' - T'_0) - \beta_S(S' - S'_0)]$.

Using a vorticity-stream function formulation, the dimensionless equations governing the fluid flow within the porous layer may be stated as follows:

$$\eta\frac{\partial\zeta}{\partial t} + \zeta = R_T\left(\frac{\partial T}{\partial x} + N\frac{\partial S}{\partial x}\right) \tag{1}$$

$$\nabla^2\psi = -\zeta \tag{2}$$

$$\frac{\partial T}{\partial t} + u\frac{\partial T}{\partial x} + v\frac{\partial T}{\partial y} = \nabla^2 T \tag{3}$$

$$\varepsilon\frac{\partial S}{\partial t} + u\frac{\partial S}{\partial x} + v\frac{\partial S}{\partial y} = \frac{1}{Le}(\nabla^2 S + M\nabla^2 T) \tag{4}$$

$$u = \frac{\partial\psi}{\partial y}; \quad v = -\frac{\partial\psi}{\partial x} \tag{5}$$

The associated dimensionless boundary conditions are

$$\left.\begin{array}{llll} x = \pm 1/2 & \psi = 0, & \dfrac{\partial T}{\partial x} = 1, & \dfrac{\partial S}{\partial x} = 1 - M \\ y = \pm A/2 & \psi = 0, & \dfrac{\partial T}{\partial y} = 0, & \dfrac{\partial S}{\partial y} = 0 \end{array}\right\} \tag{6}$$

where ζ, ψ, T and S are the dimensionless vorticity, stream function, temperature and solute concentration, respectively. The constant η is given by $\eta = \frac{C_a K\alpha}{\sigma L'^2 v}$, where C_a represents the acceleration coefficient defined in Nield and Bejan [18].

The Nusselt and Sherwood numbers, which characterize respectively, the heat and mass transfer rates, across the vertical walls, are given by

$$Nu = \frac{1}{T_{\left(\frac{1}{2},0\right)} - T_{\left(-\frac{1}{2},0\right)}} \quad \text{and} \quad Sh = \frac{1}{S_{\left(\frac{1}{2},0\right)} - S_{\left(-\frac{1}{2},0\right)}} \tag{7}$$

3. Numerical method

A standard numerical method based on a second-order finite difference approach was used to solve the governing equations. An alternating direction implicit method was used to solve the discretized transport equations. The stream function field, however, was obtained from Eq. (2) using the point successive over-relaxation method. In the horizontal (x) direction, the computation domain was divided into three regions: two regions were adjacent to the vertical walls, where the horizontal gradients were important (boundary layer regions), in which a uniform refined grid was used; and the third region was located in the centre where a coarse uniform grid was used. A similar grid strategy was used in the vertical direction. The computations reported in this paper were performed a grid size of 81×201 within the range $4 \leqslant A_r \leqslant 12$. Details concerning the numerical code validation may be found in Bourich et al. [19].

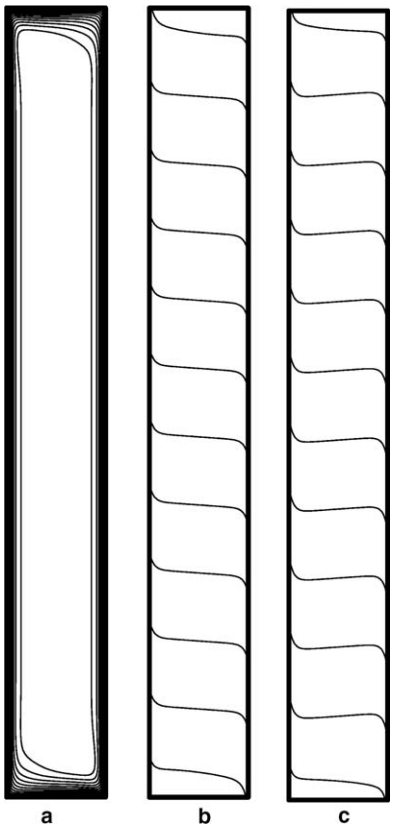

Fig. 2. Streamlines (a), isotherms (b) and concentration lines (c) obtained for $N = 3$, $M = 0.5$, $R_T = 10^3$, $Le = 3$ and $A_r = 8$.

Typical numerical results are presented in Fig. 2 in terms of the stream function (a), isotherms (b) and solute concentration contours (c). The figure shows that in the core region of the porous layer the velocity is parallel to the vertical walls while the temperature and concentration fields are linearly stratified in the vertical direction. These assumptions, which were used in the past by several authors and are confirmed numerically by Fig. 2, are the basis for the analytical solution approach developed below.

4. Analytical solution

For a sufficiently large aspect ratio enclosure ($A_r \gg 1$), the present problem can be simplified by assuming parallel flow in the central part of the cavity. This hypothesis yields the following approximations [20]:

$$\psi(x,y) = \psi(x), \quad T(x,y) = C_T y + \theta_T(x) \quad \text{and} \quad S(x,y) = C_S y + \theta_S(x) \tag{8}$$

where C_T and C_S are the unknown temperature and concentration gradients, respectively, in the y-direction. Substituting these approximations into Eqs. (1), (3) and (4), the steady simplified form of the full governing equations is transformed into a set of ordinary differential equations:

$$\frac{d^2\psi}{dx^2} = -R_T\left(\frac{d\theta_T}{dx} + N\frac{d\theta_S}{dx}\right) \tag{9}$$

$$\frac{d^2\theta_T}{dx^2} = -C_T\frac{d\psi}{dx} \tag{10}$$

$$\frac{1}{Le}\left(\frac{d^2\theta_S}{dx^2} + M\frac{d^2\theta_T}{dx^2}\right) = -C_S\frac{d\psi}{dx} \tag{11}$$

The boundary conditions in the x-direction are now given by

$$\psi = 0, \quad \frac{\partial\theta_T}{\partial x} = 1, \quad \frac{\partial\theta_S}{\partial x} = 1 - M \quad \text{for } x = \pm\frac{1}{2} \tag{12}$$

By solving the resulting ordinary differential equations (9)–(11) together with the boundary conditions (12), the solution depends on the sign of the parameter Γ, which is defined by the following expression:

$$\Gamma = R_T[C_T(1 - NM) + NLeC_S] \tag{13}$$

The present study focuses on boundary layer regime, for which $\Gamma > 0$. By setting $\Gamma = \Omega^2$ (the parameter Ω is positive), the parallel flow regime may be described by the following equations:

$$\psi(x) = A\cosh(\Omega x) + a \tag{14}$$

$$v(x) = -A\Omega\sinh(\Omega x) \tag{15}$$

$$T(x,y) = C_T y + (1 - aC_T)x - C_T A'\sinh(\Omega x) \tag{16}$$

$$S(x,y) = C_S y + [(1 - M) - a(LeC_S - C_T M)]x - (LeC_S - C_T M)A'\sinh(\Omega x) \tag{17}$$

where

$$a = \frac{R_T(1 + N - NM)}{\Omega^2}, \quad A = \frac{-a}{\cosh\left(\frac{\Omega}{2}\right)} \quad \text{and} \quad A' = \frac{A}{\Omega} \tag{18}$$

The expressions for C_T and C_S are computed using energy and mass balances across any horizontal section of the porous layer. The following expressions are obtained:

$$C_T = \frac{A_1}{1 + A_0} \quad \text{and} \quad C_S = \frac{LeA_1 - M(1 + Le)\dfrac{A_1}{1 + A_0}}{1 + Le^2 A_0} \tag{19}$$

Then, the expressions for Nusselt and Sherwood numbers are obtained as

$$Nu = \frac{1}{1 - C_T A_1} \quad \text{and} \quad Sh = \frac{1}{(1 - M) - (LeC_S - C_T M)A_1} \tag{20}$$

where

$$\begin{cases} A_0 = a^2\left[\dfrac{3}{2} - \dfrac{3}{\Omega}\tanh\left(\dfrac{\Omega}{2}\right) - \dfrac{1}{2}\tanh^2\left(\dfrac{\Omega}{2}\right)\right] \\ A_1 = a\left[1 - \dfrac{2}{\Omega}\tanh\left(\dfrac{\Omega}{2}\right)\right] \end{cases} \tag{21}$$

The combination of Eqs. (13) and (19), together with $\Gamma = \Omega^2$, leads to the following equation for Ω:

$$\Omega^2(1 + A_0 + A_0 Le^2 + A_0^2 Le^2) - R_T^2(1 + N - NM)^2\Phi(\Omega) \times \frac{1 - \dfrac{2}{\Omega}\tanh\left(\dfrac{\Omega}{2}\right)}{\Omega^2} = 0 \tag{22}$$

in which

$$\Phi(\Omega) = A_0 Le^2 + \Lambda_1 \quad \text{with } \Lambda_1 = \frac{1 + NLe^2 - NM(1 + Le + Le^2)}{1 + N - NM} \tag{23}$$

Eq. (22) has a solution only in a specific range of R_T, which depends on N, M and Le. By writing this equation in the following simplified form:

$$\Theta(\Omega) = \Theta_1(\Omega) - \Theta_2(\Omega) = 0 \tag{24}$$

where

$$\Theta_1(\Omega) = \Omega^2(1 + A_0 + A_0 Le^2 + A_0^2 Le^2) \tag{25}$$

$$\Theta_2(\Omega) = R_T^2(1 + N - NM)^2\Phi(\Omega)\frac{1 - \dfrac{2}{\Omega}\tanh\left(\dfrac{\Omega}{2}\right)}{\Omega^2} \tag{26}$$

and by studying the behaviors of functions $\Theta_1(\Omega)$ and $\Theta_2(\Omega)$ at the limits of both small and large values of Ω [21], it was found that the condition $\Phi_0 > 0$ is necessary and sufficient to obtain a solution for Eq. (22), where Φ_0 is given by

$$\Phi_0 = \frac{R_T^2(1 + N - NM)^2 Le^2}{120} + \Lambda_1 \tag{27}$$

For this case, two domains can be distinguished in the (Le, N) plane, depending on the sign of Λ_1. The first domain corresponds to $\Lambda_1 \geqslant 0$, and the condition $\Phi_0 > 0$ is satisfied regardless of the values of the governing parameters. The solution for Eq. (22) is always possible in this domain. The second domain corresponds to $\Lambda_1 < 0$, and the condition $\Phi_0 > 0$ is satisfied only when $R_T > R_{T0}$ (Le, N, M), where R_{T0} is given by the following expression:

$$R_{T0} = \left[-\frac{120}{Le^2}\frac{(1 + NLe^2 - NM(1 + Le + Le^2))}{(1 + N - NM)^3}\right]^{1/2} \tag{28}$$

This means that in the second domain, the solution for Eq. (24) exists only when R_T exceeds a critical value R_{T0}.

Hereafter, attention is focused on the boundary layer regime for which the condition $\Omega \gg 1$ must be satisfied. The boundary layer solution may be obtained as

$$\psi(x) = a\left[1 - e^{\Omega\left(|x| - \frac{1}{2}\right)}\right] \tag{29}$$

$$v(x) = \frac{|x|}{x}a\Omega e^{\Omega\left(|x| - \frac{1}{2}\right)} \tag{30}$$

$$T(x,y) = C_T y + (1 - aC_T)x + \frac{|x|}{x}\frac{aC_T}{\Omega}e^{\Omega\left(|x| - \frac{1}{2}\right)} \tag{31}$$

$$S(x,y) = C_S y + [(1 - M) - a(LeC_S - C_T M)]x + \frac{|x|}{x}\frac{a(LeC_S - C_T M)}{\Omega}e^{\Omega\left(|x| - \frac{1}{2}\right)} \tag{32}$$

and Eqs. (19) reduce to

$$C_T = \frac{a\left(1-\frac{2}{\Omega}\right)}{1+G\left(1-\frac{3}{\Omega}\right)} \quad \text{and}$$

$$C_S = \frac{aLe\left(1-\frac{2}{\Omega}\right) - M(1+Le)\left[a\left(1-\frac{2}{\Omega}\right)\right] \Big/ \left[1+G\left(1-\frac{3}{\Omega}\right)\right]}{1+GLe^2\left(1-\frac{3}{\Omega}\right)} \tag{33}$$

Then values of Nu and Sh that correspond to the boundary layer regime may be expressed as

$$Nu = \frac{1+G\left(1-\frac{3}{\Omega}\right)}{1+\frac{G}{\Omega}\left(1-\frac{4}{\Omega}\right)} \quad \text{and}$$

$$Sh = \frac{1}{[(1-M)-a(LeC_S-C_TM)]+\frac{2a(LeC_S-C_TM)}{\Omega}} \tag{34}$$

with

$$a = \frac{R_T(1+N-NM)}{\Omega^2} \quad \text{and} \quad G = a^2 \tag{35}$$

By combining Eqs. (13), (33) and (35), it is found that

$$G = a^2 = \frac{\Omega}{2C_1}\left(C_2 \pm \sqrt{C_2^2+C_3}\right) \tag{36}$$

where

$$\begin{cases} C_1 = Le^2(1+N-NM)(\Omega-3) \\ C_2 = (\Omega-3)[N+(1-NM)Le^2] \\ \qquad +NM(Le+Le^2)(\Omega-2)-(1-NM)-NLe^2 \\ C_3 = 4C_1(1+N-NM) \end{cases} \tag{37}$$

The sign of C_1 requires that only one of the two relations given by Eq. (36) may be considered to ensure that $G>0$. Therefore, an expression for G that leads to boundary layer profiles for the temperature and concentration, obtained from Eq. (36), is

$$G = d_1\Omega \quad \text{for } d_1 > 0 \tag{38}$$

where $d_1 = \dfrac{N+Le^2+NMLe}{Le^2(N+1-NM)}$.

In the (N, Le) plane and depending on the Soret parameter M, this solution exists only over the following ranges:

$$\frac{-1}{1-M} < N < \frac{-Le^2}{1+MLe} \quad \text{for } M < \frac{-1}{Le} \tag{39}$$

$$N > \max\left(\frac{-1}{1-M}, \frac{-Le^2}{1+MLe}\right)$$

or

$$N < \min\left(\frac{-1}{1-M}, \frac{-Le^2}{1+MLe}\right) \quad \text{for } \frac{-1}{Le} < M < 1 \tag{40}$$

$$\frac{-Le^2}{1+MLe} < N < \frac{-1}{1-M} \quad \text{for} \quad M > 1 \tag{41}$$

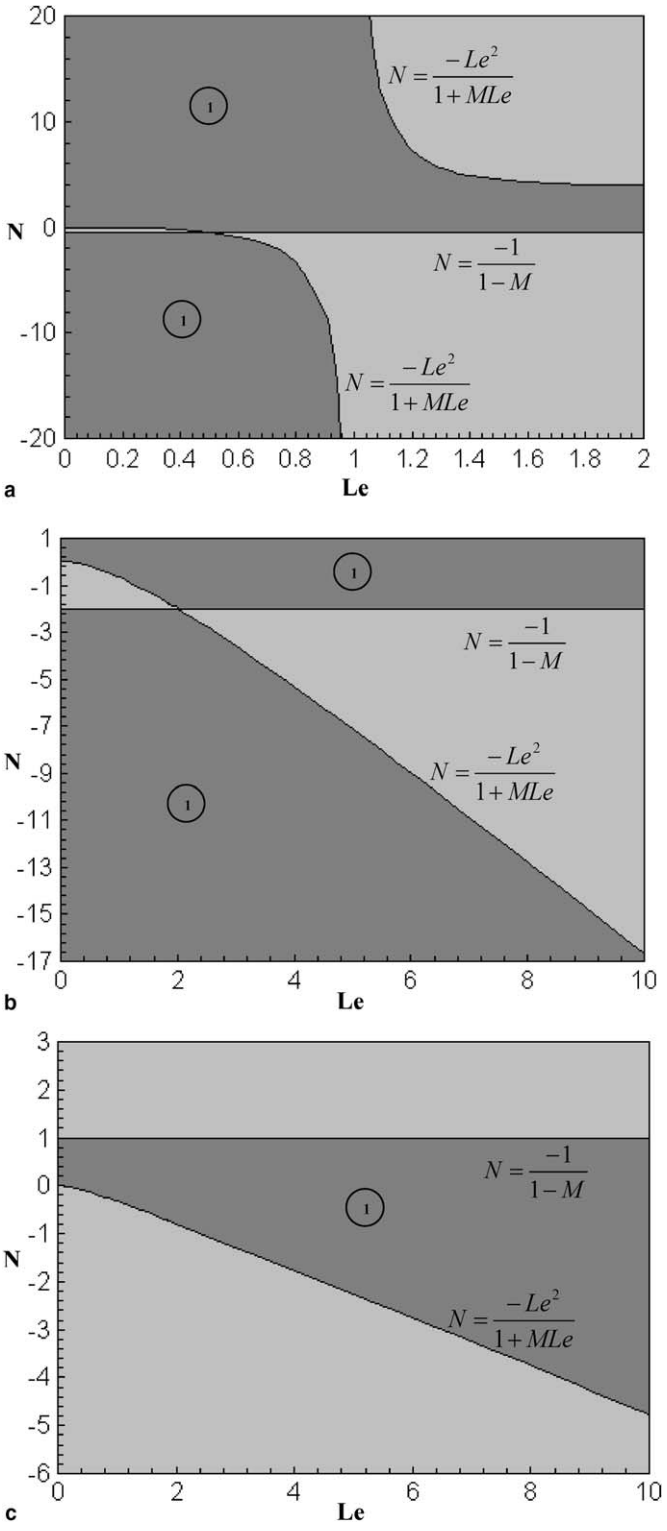

Fig. 3. Domains corresponding to different boundary layer regimes for (a) $M=-1$, (b) $M=0.5$ and (c) $M=2$.

The domain that delineates the solution ($d_1>0$) is denoted by region 1 in the (N, Le) plane. It is illustrated in Fig. 3(a)–(c) for $M=-1.0$, 0.5, and 2.0, respectively.

For sufficiently large values of R_T, Ω may be expressed in terms of R_T, N, Le and M as follows:

$$\Omega \cong R_T^{2/5}(1+N-NM)^{3/5}\left(\frac{Le^2}{N+Le^2+NMLe}\right)^{1/5} \quad (42)$$

The thickness δ of the vertical boundary layer may be deduced from this expression since δ is known to be the inverse of the parameter Ω ($\delta \propto 1/\Omega$).

5. Results and discussion

5.1. Effect of the Rayleigh number R_T

We will first focus our attention on the effect of R_T on Ω, ψ_0, Nu and Sh for given values of (N, Le) using each of the three cases corresponding to different ranges of M. From Eqs. (38) and (42), the quantities Ω and G vary as $R_T^{2/5}$. Consequently, the maximum velocity $v(x=1/2)$ varies as $R_T^{3/5}$ and the flow intensity $\psi_0 = |\psi(x=0)|$ varies as $R_T^{1/5}$. In addition, Nu and Sh vary as $R_T^{2/5}$ while C_T and C_S vary as $R_T^{-1/5}$. Therefore, the vertical gradients of both T and S decrease as R_T increases. For $x>0$, the horizontal gradients of v, T and S are expressed as

$$\frac{dv}{dx} = a\Omega^2 e^{\Omega(x-1/2)} \quad (43)$$

$$\frac{dT}{dx} = 1 + aC_T\left(e^{\Omega(x-1/2)} - 1\right) \quad (44)$$

$$\frac{dS}{dx} = (1-M) + a(LeC_S - C_T M)\left(e^{\Omega(x-1/2)} - 1\right). \quad (45)$$

According to the above equations, it can be demonstrated that the horizontal gradients of v, T and S are nearly zero outside the boundary layers regardless of the value of M, except when $M=1$ and $M=-1/Le$. This means that for high values of R_T, the horizontal profiles of v, T and S exhibit a boundary layer behavior. Furthermore, an increase in R_T tends to make the temperature and concentration more uniform in the core region of the enclosure. T and S are directly related to the parameter ρ_a, which represents the dimensionless departure of the fluid density from the reference state. For $x \neq 0$, ρ_a is given by

$$\rho_a = -(T+NS) = -(C_T + NC_S)y - \frac{|x|}{x}\frac{(1+N-NM)}{\Omega}e^{\Omega(|x|-1/2)} \quad (46)$$

The above equation clearly shows that for large R_T, both the horizontal and vertical density gradients become zero outside the boundary layer, which indicates that the horizontal profile of ρ_a also exhibits a boundary layer behavior. As a result, an increase in R_T also tends to make the density more uniform in the core region of the enclosure. Furthermore, when $|N|$ is sufficiently small ($|N| \ll |Le^2/(1+MLe)|$), the expression for Ω defined by Eq. (42) reduces to

$$\Omega \cong (R_T^2(1+N-NM)^3)^{1/5} \quad (47)$$

The expressions for Ω, Nu and Sh may be examined for two important limiting cases that can be recovered by the present formulation. The first one corresponds to the thermally-driven boundary layer flow regime, in which the thermal buoyancy effect dominates, i.e., $|N| \ll |1/(1-M)|$. For this situation, $\Omega \cong R_T^{2/5}$, and the expressions for Nu and Sh given in Eq. (34) reduce to

$$Nu \cong \frac{\Omega}{2}, \quad Sh \cong \frac{1}{1-M}\left(\Omega + \sum_{i=0}^{2}\left(\frac{4}{\Omega}\right)^i\right) \quad \text{for } Le \gg 1 \quad (48)$$

and

$$Nu \cong \frac{\Omega}{2}, \quad Sh \cong \frac{1}{1+MLe}\left(1 + Le^2\Omega\left(1-\frac{3}{\Omega}\right)\right) \quad \text{for } Le \ll 1 \quad (49)$$

The second limiting case corresponds to the solutably-driven boundary layer flow regime, where the flow is dominated by the solutal buoyancy force, i.e., $|N| \gg |1/(1-M)|$ and ($|N| \gg |Le^2/(1+MLe)|$). For this case, Ω can be expressed in terms of the solutal Darcy–Rayleigh number, R_S, as

$$\Omega \cong R_S^{2/5}(1-M)^{3/5}(1+MLe)^{-1/5} \quad (50)$$

where $R_S = R_T Le|N|$.

Under these conditions, the expressions for both Nu and Sh may be approximated by

$$Nu \cong 1 + d_1(\Omega - 4), \quad Sh \cong \left(\frac{1}{Sh_0} + M\left(\frac{1}{1+\eta_2\Omega} + \frac{1}{1+\eta_3\Omega}\right)\right)^{-1} \quad \text{for } Le \gg 1 \quad (51)$$

and

$$Nu \cong 1 + \eta_4\Omega + 4\frac{\eta_4}{\Omega}, \quad Sh \cong \frac{\Omega}{(1/\eta_1) + M(1/\eta_5)} \quad \text{for } Le \ll 1 \quad (52)$$

where $Sh_0 \cong 1 + 4\eta_1(\eta_1 - 1) + \eta_1\Omega$ and

$$\eta_1 = \frac{d_1 Le^2}{1+d_1 Le^2}, \quad \eta_2 = \frac{d_1 Le^2}{3d_1 Le^2 - 1}, \quad \eta_3 = \frac{d_1 Le}{1-4d_1 Le},$$
$$\eta_4 = \frac{d_1}{1+d_1} \quad \text{and} \quad \eta_5 = \frac{d_1 Le}{1-d_1 Le}.$$

It should be noted that in the absence of the Soret effect, a situation that corresponds to $M=0$, Eqs. (47)–(52) lead to expressions identical to those obtained previously by Mamou et al. [22] for $d_1 > 0$ while studying a pure double-diffusive problem with the same configuration.

We now turn our attention to the effect of R_T on Ω, ψ_0, Nu and Sh for given values of N, Le and M. The variations of Ω with R_T are illustrated in Fig. 4(a)–(c) for different values of M and different combinations of (N, Le) satisfying the condition $d_1 > 0$. For a given value of M, the figure shows that the boundary layer analytical approximation given by Eq. (42) (presented with dotted lines in the figures) agreed well with the parallel flow solution for relatively large values of R_T. The critical values of R_T beyond which the boundary layer regime was achieved depended on the parameters M, N and Le. Thus, by considering the case in Fig. 4(a) that corresponds to $M=-0.5$, good agreement

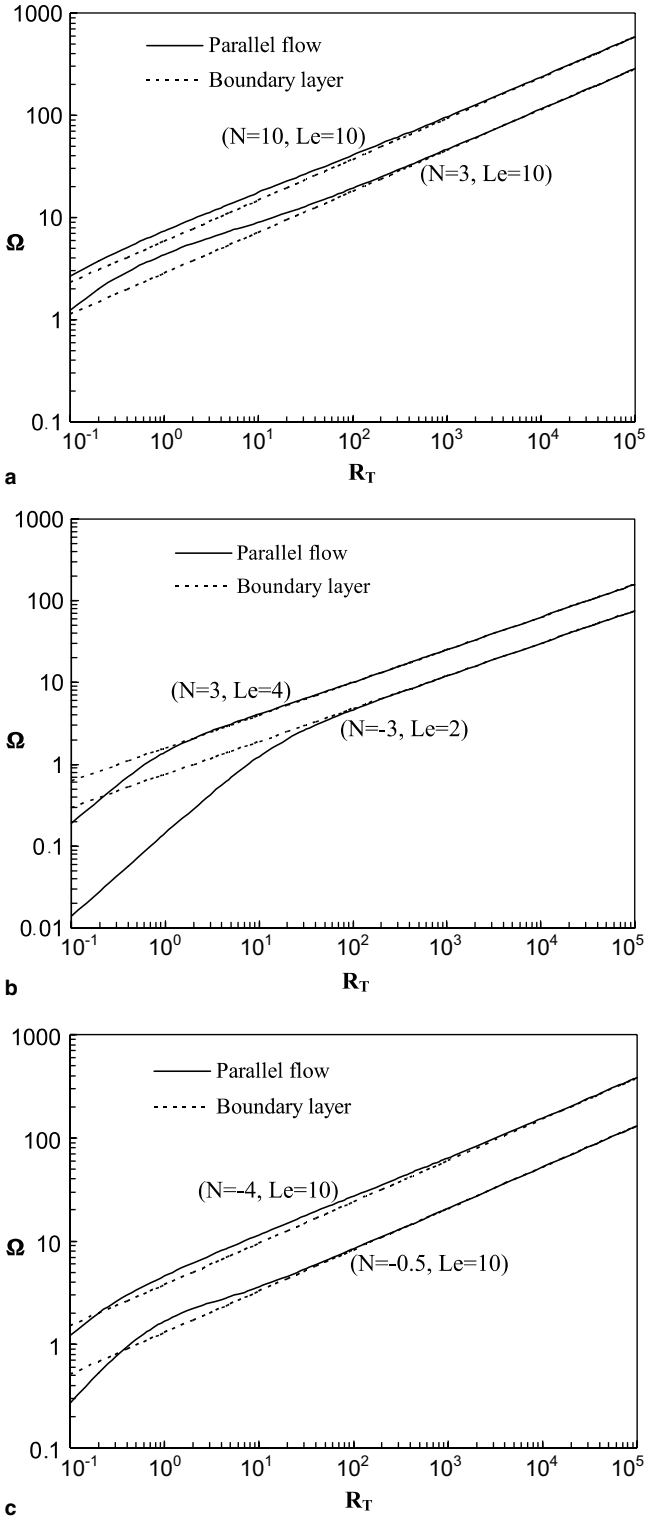

Fig. 4. Effect of R_T on Ω for (a) $M = -0.5$, (b) $M = 0.5$ and (c) $M = 2$ and different combinations (N, Le).

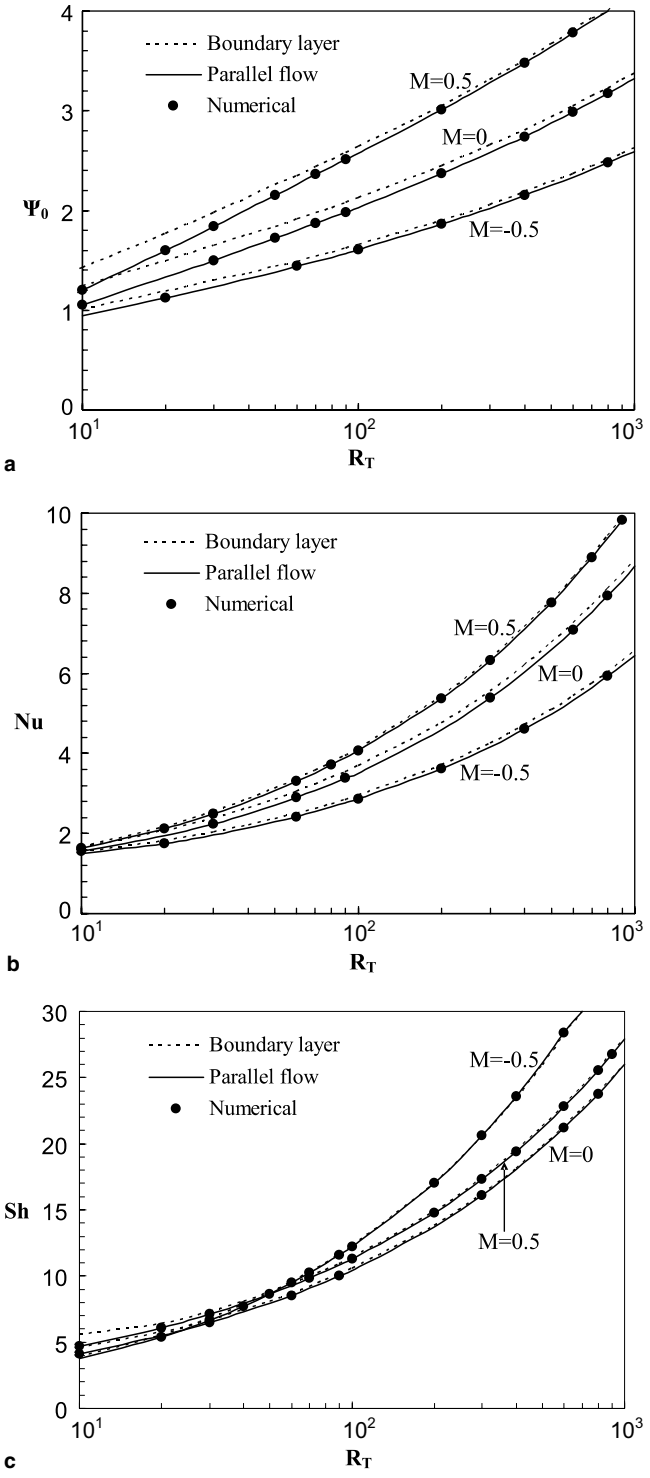

Fig. 5. Effect of R_T on (a) ψ_0, (b) Nu and (c) Sh for $(Le, N) = (3, 3)$ and different values of M.

was obtained for $R_T > 80/(>250)$ when $(N, Le) = (3, 10)/(10, 10)$. The results presented in this figure also prove that the thickness of the vertical boundary layer, δ, decreased monotonically with R_T. This trend is in agreement with the analytical predictions, where δ varied according to $R_T^{-2/5}$.

The evolution of the flow intensity, ψ_0, Nusselt number, Nu, and Sherwood number, Sh, with R_T are displayed in Fig. 5(a)–(c) for $(Le, N) = (3, 3)$ and different values of M (0 and ± 0.5). The boundary layer regime was reached at sufficiently large values of R_T. These results support the analytical approximations used for the boundary layer regime ($\Omega \gg 1$) and, at the same time, assess the validity

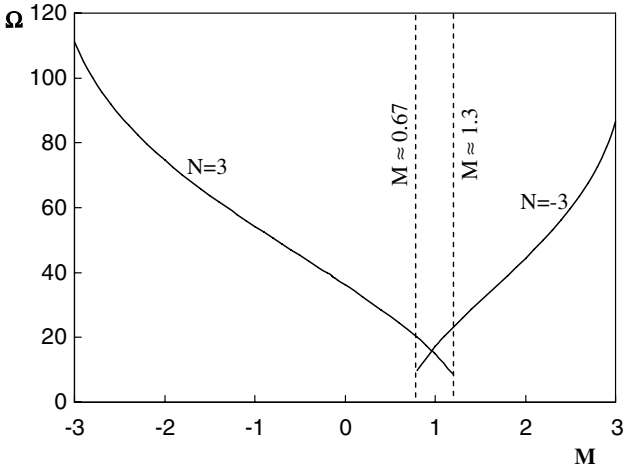

Fig. 6. Effect of M on Ω for $Le = 10$, $R_T = 10^3$ and different values of N.

of the analytical parallel flow solution when compared against the numerical results obtained by solving the full governing equations.

5.2. Effect of M

The effect of the Soret parameter, M, on the flow intensity, ψ_0, and Nusselt number, Nu, is illustrated in Fig. 5(a) and (b). For a given value of R_T, the Soret parameter, M, varied within the range $-0.5 \leqslant M \leqslant 0.5$, leads to an increase in ψ_0 and Nu for $(N, Le) = (3, 3)$.

The Soret effect on the boundary layer thickness (through the parameter Ω) was also studied for given combinations of Le, N and R_T. The variations of Ω with M in the boundary layer regime are illustrated in Fig. 6 for $Le = 10$, $R_T = 10^3$ and $N = \pm 3$. According to the analytical results, the Soret effect on the boundary layer thickness, δ, depended on the sign of N. For a positive/negative value of N, δ increased/decreased monotonically as M increased. For the case $N = 3$, or for $N > 0$ in general, the Soret effect induced an increase in the boundary layer thickness when M increased within the range $-3.4 < M < 1.3$ for $N = 3$, provided that d_1 remained positive. For the case $N = -3$, the boundary layer regime considered in this study existed only when the parameter M exceeded a critical value, M_{CR}, given analytically by $M_{CR} = (N + 1)/N$ ($M_{CR} \cong 0.67$ for $N = -3$). The effect of the Soret parameter was characterized by a decrease in the boundary layer thickness for the case of opposing thermal and solutal buoyancy forces ($N < 0$). The approximate expression of Ω given in Eq. (47) was validated for the case $N = 3$ when $M = -0.2$. For these values, the simplified Eq. (47) gave a value of $\Omega = 39.59$, which agrees very well with the value 39.83 predicted by the boundary layer solution given by Eq. (42).

6. Conclusions

The Soret effect on double-diffusive convection induced in a vertical porous layer, subject to horizontal heat and mass fluxes, was investigated analytically and numerically in the limit of the boundary layer regime. The analytical solution based on the parallel flow approximation was validated numerically. It was demonstrated that there existed several domains in the (N, Le) plane with different boundary layer regime behaviors, depending on the Soret parameter. For a given value of M, the horizontal profiles of temperature and solute concentration exhibited boundary layer behaviors only in some regions within the (N, Le) plane. The Soret parameter had a strong effect on the vertical boundary layer thickness. The boundary layer thickness increased with the Soret parameter when the thermal and solutal buoyancy forces are cooperating ($N > 0$); however, the boundary layer thickness decreased with the Soret parameter when the thermal and solutal buoyancy forces opposed each other ($N < 0$).

References

[1] C. Karcher, U. Müller, Bénard convection in binary mixture with a nonlinear density–temperature relation, Phys. Rev. E 49 (1994) 4031–4043.
[2] A. Mansour, A. Amahmid, M. Hasnaoui, M. Bourich, Soret effect on double-diffusive multiple solutions in a square porous cavity subject to cross gradients of temperature and concentration, Int. Comm. Heat Mass Transfer 31 (2004) 431–440.
[3] M. Bourich, M. Hasnaoui, A. Amahmid, M. Mamou, Soret driven thermosolutal convection in a shallow porous enclosure, Int. Comm. Heat Mass Transfer 29 (2002) 717–728.
[4] O. Sovran, M.C. Charrier-Mojtabi, A. Mojtabi, Naissance de la convection thermo-solutale en couche poreuse infinie avec effet Soret, C.R. Acad. Sci. Paris 329 (2001) 287–293.
[5] M. Er-Raki, M. Hasnaoui, A. Amahmid, M. Bourich, Soret driven thermosolutal convection in a shallow porous layer with a stress-free upper surface, Engng. Comput. 22 (2005) 186–205.
[6] A. Bahloul, N. Boutana, P. Vasseur, Double-diffusive and Soret-induced convection in a shallow horizontal porous layer, J. Fluid Mech. 491 (2003) 325–352.
[7] S.M. Alex, P.R. Patil, Effect of variable gravity field on Soret driven thermosolutal convection in a porous medium, Int. Comm. Heat Mass Transfer 28 (2001) 509–518.
[8] M. Bourich, M. Hasnaoui, A. Amahmid, M. Mamou, Soret convection in a shallow porous cavity submitted to uniform fluxes of heat and mass, Int. Comm. Heat Mass Transfer 31 (2004) 773–782.
[9] M. Bourich, M. Hasnaoui, M. Mamou, A. Amahmid, Soret effect inducing subcritical and Hopf bifurcations in a shallow enclosure filled with a clear binary fluid or a saturated porous medium: a comparative study, Phys. Fluids 16 (2004) 551–568.
[10] M. Marcoux, M.C. Charrier-Mojtabi, A. Bergeon, Naissance de la thermogravitation dans un mélange binaire imprégnant un milieu poreux, Entropie 214 (1998) 31–36.
[11] L.B. Benano-Melly, J.-P. Caltagirone, B. Faissat, F. Montel, P. Costeseque, Modeling Soret coefficient measurement experiments in porous media considering thermal and solutal convection, Int. J. Heat Mass Transfer 44 (2001) 1285–1297.
[12] F. Joly, P. Vasseur, G. Labrosse, Soret instability in a vertical Brinkman porous enclosure, Numer. Heat Transfer, Part A: Appl. 39 (2001) 339–359.
[13] N. Boutana, N. Bahloul, P. Vasseur, F. Joly, Soret and double diffusive convection in a porous cavity, J. Por. Media 7 (2004) 41–57.
[14] O.V. Trevisan, A. Bejan, Natural convection with combined heat and mass transfer buoyancy effects in a porous medium, Int. J. Heat Mass Transfer 28 (1985) 1597–1611.

[15] O.V. Trevisan, A. Bejan, Mass and heat transfer by natural convection in a vertical slot filled with porous medium, Int. J. Heat Mass Transfer 29 (1986) 403–415.
[16] F. Alavyoon, On natural convection in vertical porous enclosures due to prescribed fluxes of heat and mass at the vertical boundaries, Int. J. Heat Mass Transfer 36 (1993) 2479–2498.
[17] A. Amahmid, M. Hasnaoui, M. Mamou, P. Vasseur, Boundary layer flows in a vertical porous enclosure induced by opposing Buoyancy Forces, Int. J. Heat Mass Transfer 42 (1999) 3599–3608.
[18] D.A. Nield, A. Bejan, Convection in Porous Media, second ed., Springer, New York, 1999.
[19] M. Bourich, A. Amahmid, M. Hasnaoui, Double-diffusive convection in a porous enclosure submitted to cross gradients of temperature and concentration, Energy Convers. Manage. 45 (2004) 1655–1670.
[20] D.E. Cormack, L.G. Leal, J. Imberger, Natural convection in a shallow cavity with differentially heated end walls, Part 1: asymptotic theory, J. Fluid Mech. 65 (1974) 209–230.
[21] A. Amahmid, M. Hasnaoui, M. Mamou, P. Vasseur, On the transition between aiding and opposing double diffusive flows in a vertical porous matrix, J. Por. Media 3 (2) (2000) 123–137.
[22] M. Mamou, P. Vasseur, E. Bilgen, D. Gobin, Double-diffusive convection in an inclined slot filled with porous medium, Eur. J. Mech. B/Fluids 14 (1995) 629–652.